Bioactive nonthermal biocompatible plasma enhances migration on human gingival fibroblasts

Bioactive Non-Thermal Biocompatible Plasma Enhances Migration on Human Gingival Fibroblasts

Ihn Han[1,2¶], In-Seok Song[3¶], Seung Ah Choi[4], Taebok Lee[5], Maksudbek Yusupov[6], Priyanka Shaw[6], Annemie Bogaerts[6], Eun Ha Choi[1*], and Jae Jun Ryu[3*]

[1]Plasma Bioscience Research Center, Applied Plasma Medicine Center, Kwangwoon University, Seoul, 01897, Republic of Korea

[2]Department of Plasma Bio-Display, Kwangwoon University, Seoul 01897, Korea

[3]Department of Dentistry, Korea University Anam Hospital, Seoul, 02841, Republic of Korea

[4]Division of Pediatric Neurosurgery, Pediatric Clinical Neuroscience Center, Seoul National University Children's Hospital, Seoul, 03080, Republic of Korea.

[5]Confocal Core Facility, Center for Medical Innovation, Seoul National University Hospital, Seoul 03082, Korea

[6]Research group PLASMANT, Department of Chemistry, University of Antwerp, Universiteitsplein 1, B-2610 Antwerp, Belgium

[*]Corresponding author: Eun Ha Choi, Ph.D.

Plasma Bioscience Research Center, Kwangwoon University, Gwangun-ro 20, Nowon-gu, Seoul, 139-701, Republic of Korea, Tel.: +82-2-940-5661, Fax: +82-2-960-5664; E-mail: ehchoi@kw.ac.kr

[*]Corresponding author: Jae Jun Ryu, DDS, MSD, PhD

Department of Prosthodontics, Korea University Anam Hospital, 73, Inchon-ro, Seongbuk-gu, Seoul, 02841, Republic of Korea, Tel.: +82-2-920-5423, Fax: +82-2-921-7348; E-mail: koprosth@unitel.co.kr

¶ These authors contributed equally to this work.

Abstract

This study hypothesized that the application of low-dose non-thermal biocompatible dielectric barrier discharge plasma (DBD-NBP) to human gingival fibroblasts (HGFs) would inhibit colony formation but not cell death and induce matrix metalloproteinase (MMP) expression, extracellular matrix (ECM) degradation, and subsequent cell migration, which could result in enhanced wound healing. HGFs treated with plasma for 3 min migrated to each other across the gap faster than those in the control and 5-min treatment groups on days 1 and 3. The plasma-treated HGFs showed significantly high expression levels of the cell cycle arrest-related *p21* gene and enhanced MMP activity. FAK-mediated attenuation of wound healing or actin cytoskeleton rearrangement, and plasma-mediated reversal of this attenuation supported the migratory effect of DBD-NBP. Further, we performed computer simulations to investigate the effect of oxidation on the stability and conformation of the catalytic kinase domain of FAK. We found that the oxidation of highly reactive amino acids Cys427, Met442, Cys559, Met571, Met617, and Met643 changes the conformation and increases the structural flexibility of the FAK protein and thus modulates its function and activity. Low-dose DBD-NBP-induces host cell cycle arrest, ECM breakdown, and subsequent migration, thus contributing to the enhanced wound healing process.

Keywords: non-thermal biocompatible plasma, oral wound healing, migration, focal adhesion kinase signaling, catalytic kinase domain

1. Introduction

Plasma is defined as an ionized gas consisting of charged particles (electrons and ions), radicals, stimulated atoms and molecules, and visible and UV photons [1]. This complex mixture can be applied to a variety of fields. Recently developed non-thermal biocompatible plasma (NBP), which uses ambient air and is conducted at a temperature lower than 40 °C, can be used in various biomedical applications [2], for example, for killing bacteria, viruses, and fungi, and even cancer cells [3–7], sterilizing wounds [8], and enhancing wound healing [9]. It is also widely used for oral bacterial inactivation [10] and tooth whitening [11].

The direct effects of NBP on cells are derived from highly reactive, short-acting radicals, including reactive oxygen species (ROS) and reactive nitrogen species (RNS) [12]. These ROS/RNS have double-sidedness, which means that their short-time, low dosage stimulates cell viability, proliferation, and migration, but their long-time, high dosage induces cell senescence or apoptosis by oxidative damage in mitochondrial DNA, proteins, and lipids [13–16]. The effects of NBP could also be mediated by indirect factors, such as electric

or magnetic field, temperature, pH effects, UV radiation, or osmolality change [17]. The positive action of NBP may be explained by the synergistic effect of the various factors mentioned above [18].

NBP has a variety of available sources with various physical and chemical properties, such as direct floating electrode-DBD (FE-DBD), indirect jet plasma, and hybrid-type plasma based on the surface microdischarge technique [1]. The formation of plasma products can also be modified by several factors, including treatment time, gas applied (oxygen, nitrogen, argon, or helium), application type (direct or indirect), cell adherence (adherent or suspension), cell type (keratinocyte, endothelial cell, or fibroblast), differential voltage, and gas flow rate [1,19].

Among them, non-thermal DBD plasma is useful for its transportability, scalable function, controllability, and cost-benefit [20]. The DBD is defined as a discharge between two electrodes insulated by a dielectric barrier [21]. The dielectric barrier enables microdischarge between the gaps filled with atmospheric air or gas, which is high enough to cause ozone generation, disinfection, or pollution control. The DBD, using the human body as a counter electrode, primarily provides a more homogenous yield of plasma and plasma-driven species than indirect plasma sources [22].

Plasma medicine has evolved from an obscure and little-accepted medical specialty to one that is critical to both clinical care and medical research in recent years. There are currently plasma sources specifically intended for the treatment of wound healing illnesses, and research into the cellular pathways mediated by plasma therapy in wound healing is well underway. However, switching from one plasma device to another will not result in the same therapeutic benefits. The biological effects caused by ROS, RNS radiation, working gas flow, electrical current flow from plasma to the body, and heat transfer to the treated surface, according to the plasma generating technology and its components, are the reason for this non-transferability. For wound healing, NBP has been successfully applied in patients with chronic wounds, such as chronic venous ulcers [8], and is thought to primarily act by killing bacteria and blocking bacteria-driven delayed wound healing. However, whether this effect is primarily due to a decrease in bacterial colonization or direct stimulating effects on cells is still unclear. The potential of NBP to stimulate tissue regeneration and render microbiological organisms insert makes it useful for wound treatment. The NBP-treated patients had a significant reduction in the length of time required for tissue healing, no infection or postoperative pain, and almost immediate return of oral functions; they did not require analgesics. Following a biopsy of the mobile oral mucosa, wound administration of NBP may be advised as a safe and dependable alternative for healing tissue in wounds. NBP improved wound healing by promoting re-epithelialization, wound closure, the late phase of inflammation, and boosting tissue repair strength and rate of maturity. NBP therapy for acute wounds may hasten wound closure,

prevent or cure wound infection, and contribute to a better-quality scar in terms of strength and visual appearance. A quicker healing time can minimize costs, discomfort, hospitalization, and problems during the healing phase, and enhance the patient's quality of life. Furthermore, not enough studies have dealt with the effects of NBP on the acute wound healing process and unveiled a clear signaling mechanism for wound healing [23].

Therefore, the present study investigated whether non-thermal DBD plasma supplied with dry air would take a positive role in the wound healing process. This study hypothesised that non-thermal biocompatible DBD plasma (DBD-NBP) would accelerate the migration of the HGFs and result in improved wound healing.

2. Materials and Methods

2.1. Non-thermal DBD plasma generator with air supply

A round DBD plasma generator of 35 mm diameter was specially designed for plasma application to cells in a 35-mm dish. Dry air was supplied during plasma generation within a sealed chamber [Figure 1(a)]. An alternating current was generated with 25 ms on-time, 175 ms off-time, 1.69 kV, and 9.6 mA (Table 1, Figure 1(b)). The optical emission spectrum peaked at 330 nm [Figure 1(c)].

2.2. Isolation and expansion of HGFs from gingival tissue

HGFs were obtained from the gingival tissue of healthy human donors, as previously described [24,25], under the approval of the Institutional Review Board (IRB) of Korea University Anam Hospital (IRB No. ED14167). All experiments were performed in accordance with the relevant guidelines and regulations of the IRB of Korea University Anam Hospital. Written informed consent was obtained from all participants, before using their gingival tissues in this study. The gingival tissues were immersed in sterile Hanks' balanced salt solution supplemented with penicillin (200 units/mL) and streptomycin (200 g/mL). The tissues were washed twice with Ca^{2+}- and Mg^{2+}-free Dulbecco's PBS (DPBS) and then exposed to 3 mg/mL type I collagenase for 1 h at 37 °C. Subsequently, the tissues were centrifuged at 2,500 rpm for 20 min and then washed and resuspended in PBS. The isolated cells, referred to as HGFs, were filtered through a 100 μM cell strainer (BD, catalog no. 352360) and cultured in α-MEM containing 10 % FBS and 1 % antibiotics, and the medium was changed every 2–3 days. All experiments were performed in passages # 3–8.

2.3. Cell viability

Cell viability was measured by the MTS assay (Promega, Madison, WI), according to the manufacturer's instructions. The HGF cells were seeded into culture plates at a concentration of 2×10^5 cells/35-mm culture dish in 2 mL of alpha-MEM media and cultured overnight. After treatment with DBD-NBP at a different time, the cells were incubated for 24 h and then treated with the MTS reagent for 4 h. All supernatant samples were transferred to a 96-well plate and read at 490 nm using a microplate reader (Biotek, VT, USA).

For the ATP activity assays, cells were plated in a 35-mm culture dish in the same conditions as for the MTS assay. After 24 h, cells were lysed with the CellTiter-Glo Luminescent Cell Assay Kit (Promega), and luminescence was read using a microplate reader (Biotek).

Live/dead staining was performed using an assay kit (Molecular probes, USA). Cells were treated with plasma for 3, 5, and 10 min. The working gas effect was eliminated by performing an only-gas treatment for 5 and 10 min in cells without plasma discharge. After 24 h of treatment, cells were stained with 4 μM of EthD-1 and 2 μM of calcein AM and incubated for 20 min at room temperature in the dark. Images of the cells were captured using a fluorescence microscope (Nikon, USA).

2.4. Colony formation assay

The isolated HGF cells were first investigated by performing a colony formation assay, using a method described previously [25]. The cells were plated at a density of 1×10^2 cells per mm^2 and maintained for 15 days at 37 °C. The DBD-NBP was applied at 2 L/min for 3 min at each time point to the cells in all experimental groups. Thereafter, the cells were fixed and stained in 4 % paraformaldehyde solution for 10 min, washed with DPBS, and then stained with 0.1 % crystal violet for 10 min. It was considered as colony forming units-fibroblast when more than 50 cells with a fibroblast phenotype were aggregated. The absorbance of crystal violet was read at 375 nm on a microplate reader, Synergy™HT (BioTek).

2.5. In vitro wound healing assay

An initial 4 x 10^5 cells were seeded in both wells of a 35 μm-dish (ibidi® Culture-Insert 2 Well, GmbH, Martinsried, Germany) for performing a two-dimensional invasion assay. After 24 h in culture medium (DMEM), serum was removed, and cells were immediately time-dependently treated with non-thermal DBD plasma for 3 and 5 min. Both confluent plates of HGF cells were removed after 24 h, and the cells invading the gap (500 μm) were subsequently monitored under a microscope (Nikon Eclipse Ti, Japan). Thereafter, the wound closure rate was determined by measuring the area of the open wound at each time point relative to the

area of the wound at the time of wounding using the TScratch® software program (CSElab, Zurich, Switzerland) [26].

2.6. Detection of reactive species

For ROS/RNS detection, we used 2′7′-dichlotodihydrofluorescein diacetate (H_2DCFDA; Invitrogen, CA, USA) for intracellular ROS level detection, QuantiChrom™ Peroxide Assay Kit for H_2O_2 detection, and QuantiChrom™ Nitric Oxide Assay Kit (BioAssay Systems, CA, USA) for intracellular RNS level detection. The experiments were performed according to the manufacturer's protocol. Cells were treated with DBD-NBP for 3 and 5 min. Non-treated cells were used as a negative control, and cells treated with 100 μM of H_2O_2 were used as a positive control for H_2O_2 detection. To investigate intracellular ROS, 24 h after treatment, cells were loaded with 20 μM H_2DCFDA and incubated for 30 min in dark conditions. Subsequently, the cells were washed twice with PBS to remove the extra H_2DCFDA, and each group of cells was collected and analyzed in a flow cytometer (BD Biosciences). H_2O_2 detection was performed according to the manufacturer's protocol. Briefly, the samples and substrate were incubated for 30 min at room temperature and optical density (OD) was read at 585 nm. The concentration of H_2O_2 was calculated according to the standard curve (plotted using H_2O_2 solution at the standard concentrations of 0, 3, 6, 9, 12, 18, 24, and 36 μM). For RNS detection, we used a microplate reader to read the absorbance at OD 540 nm of the samples incubated with the substrate for 10 min at 60 °C. As final products of NO decomposition in the solution, the concentrations of NO_2^- and NO_3^- were calculated according to the standard curve (plotted using NO_2^- and NO_3^- at the standard concentrations of 0, 30, 60, and 100 μM, respectively).

2.7. Quantification of gene expression related to HGF migration

Total RNAs were extracted from frozen cells using the RNeasy Plus Kit (Qiagen NV, Hilden, Germany). Complementary DNAs (cDNAs) were synthesised with the Transcriptor First Strand cDNA Synthesis Kit (Roche Diagnostics GmbH, Mannheim, Germany) using a random hexamer. These cDNA samples were then analyzed using SYBR Green I Master Mix on the LightCycler® 480II (Roche). The results were normalized using the human beta-actin gene as a control. PCR was performed with the related primers for MMP-2, VEGF, Collagen type I, Collagen type IV, PDGF-beta, CDKN1A (p21), and beta-actin (Supplementary information).

2.8. Zymography for the detection of MMP-2/9 activation

A zymographic analysis was carried out in 8 % (w/v) SDS-polyacrylamide gels containing gelatin (1.5 mg/ml), as previously described (ref. number: PMID: 22144310). The gels were stained and destained with SimplyBlue SafeStain (Invitrogen™, Thermo Fisher Scientific, MA, USA), according to the manufacturer's procedure. Zones of enzymatic activity were photographed using Printgraph 2M (ATTO Co., LTD., Tokyo, Japan).

2.9. Immunoblot analysis

Immunoblot analysis was conducted as described (Supplementary information). Antibodies against AKT (Cat. #4691), p-AKT-S473 (Cat. #4060), mTOR (Cat. #2972), p-mTOR-S2448 (Cat. #2971), and p-FAK(Y397) (Cat. #3283S) were purchased from Cell Signaling Technology (MA, USA). Antibodies against p21 (Cat. sc-152), VEGF (Cat. sc-152), and GAPDH (Cat. sc-32233) were purchased from Santa Cruz Biotechnology (CA, USA). The ImageJ software program (National Institutes of Health, USA) was used for the quantification of immunoblot results. The phosphorylated proteins were normalized with GAPDH.

2.10. Confocal fluorescence imaging of HGF morphology

HGF cells were seeded on the sterilized cover glass and treated with plasma for 3 min, with or without FAK inhibitor (PF-562271, Selleckchem, Houston, TX, USA) cultured for 72 h, and then fixed using 4% paraformaldehyde. The localization of F-actin was determined using Phalloidin Alexa-488 (Abcam, Germany), and cell nuclei were stained with Hoechst 33342 (Bio-Rad, CA, USA) according to the manufacturer's instructions. Representative images were taken using the biological confocal laser scanning microscope OFV10-ASW (Olympus, Hamburg, Germany).

2.11. Computational details

Molecular dynamics (MD) simulations were carried out to study the effect of oxidation on the kinase domain (KD) of the FAK protein (PDB ID: 4K9Y (6)). For this purpose, we prepared two model systems, i.e. the native KD and its oxidised form, illustrated in Figure S1 of the Supplementary Information. All simulations were performed at 310 K and 1.0 bar, employing a V-rescale thermostat with a time constant of 0.1 ps [27] and a Parrinello-Rahman barostat with a time constant of 2.0 ps [28]. A cutoff of 1.4 nm was used for non-bonded (i.e. van der Waals and Coulomb) interactions, and the electrostatics were treated with the reaction field method [29]. In all simulations, a time step of 2 fs was used, and the MD trajectories were saved every 100 ps. Periodic boundary conditions were applied in all directions. Thus, we prepared three replicas of the native and oxidised

KD systems with different initial velocities, generating a total of six structures. These model systems were utilised to calculate the average RMSD values of the alpha carbons of the KD protein before and after oxidation. Furthermore, we used these systems to determine the secondary structures of the native and oxidised KD proteins during the last 50 ns of the equilibration. The SASA of each AA residue in the native KD protein was also calculated in the last 50 ns of the equilibration to identify the AAs highly exposed to the solvent. These AAs were then considered to create the oxidised KD structure. Specifically, the KD system was oxidised through the modification/oxidation of the Met and Cys residues that had higher SASA values and were highly reactive to the plasma treatment according to literature [30,31] (see also Tables S1 and S2 in the Supplementary Information).

All MD simulations were carried out using the GROMACS 5.1.2 package [32], employing the GROMOS 54A7 force field [33]. The parameter set of the oxidised Met and Cys residues used in the oxidised KD was obtained from [34]. The SASAs and secondary structures of the native and oxidised KD proteins were calculated with the gmx sasa and gmx do_dssp tools of GROMACS, respectively, using the data obtained from 500 snapshots of the MD trajectory taken at every 100 ps from the last 50 ns and averaging over three replicas.

2.12. Statistical analysis

Statistical analyses were performed using a two-tailed Student's *t*-test. The statistically significant differences were based on **P*-value <0.05, ***P*-value < 0.01, ****P*-value < 0.001. All experiments were replicated in triplicate, and the data are represented by the mean ± standard deviation of replicates.

3. Results

3.1. NBP-generated DBD plasma device

NBP was generated by a DBD plasma device that used air gas as a feeding gas in this study. The properties of this device have been well described in our previous study [35]. Figure 1 shows the optical emission spectra of NBP that were measured by charge-coupled device spectrometry (HR400, Ocean Optics, Dunedin, FL), while the current and voltage were measured by an oscilloscope (Tektronix, Beaverton, OR).

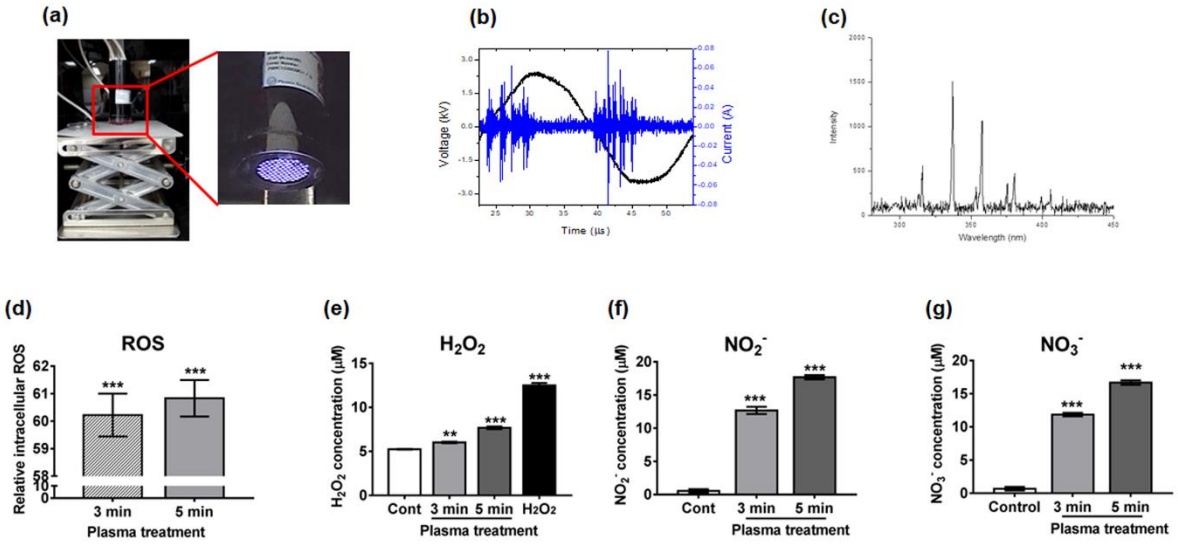

Figure 1. Dielectric barrier discharge (DBD) plasma source. (a) Application of plasma to the cells on a 35-mm-diameter dish using a discharging plasma source. (b) Electric characteristics. (c) The optical emission spectrum of non-thermal biocompatible plasma (NBP). Total intracellular reactive oxygen species (ROS) level in human gingival fibroblasts (HGFs) after treatment with air-plasma for 3 and 5 min at the rate of 2 L/min, 25 ms on-time, and 150 ms off-time. (d) Total intracellular ROS level (sample/control), (e) H2O2 concentration, (f) Nitrite concentration and (g) Nitrate concentration, Control means the gas-only treatment.

3.2. Intracellular ROS and RNS levels in HGFs after treatment with NBP-DBD plasma

Intracellular ROS and RNS levels were evaluated following NBP treatment for 3 and 5 min, respectively (Figure 1(d)). After day 1, the intracellular ROS levels of the 3- and 5-min-treated groups increased significantly over those of the control group (p-value<0.001). The concentration of hydrogen peroxide (H_2O_2) also increased in groups of 3- and 5-min NBP treatment compared to the gas-only treatment (control) group [Figure 1(e)]. Next, nitrite and nitrate concentrations were measured to estimate the RNS levels. Both nitrite (Figure 1(f)) and nitrate levels (Figure 1(g)) within the cells significantly increased to (12.04 ± 0.03) % and (11.92 ± 0.026) % for 3 min, and (17.03 ± 0.04) % and (16.85 ± 0.041) % for 5 min, respectively, compared with the control [(0.71 ± 0.01) % and (0.7 ± 0.08) %)] levels in HGFs, according to the exposure time of NBP.

3.3. Effects of NBP on the viability and colony formation ability of HGFs

The effect of NBP on the viability of HGFs was assessed according to the exposure time via the MTS tetrazolium assay. The HGFs were stable in their viability with up to 300 s of air-plasma treatment at 2 L/min, 25 ms on-time, and 150 ms off-time. Later, the effect of NBP on HGFs was confirmed by the adenosine

triphosphate (ATP) assay. The results showed that ATP as the energy currency of HGFs was elevated until 60 s, and it was stable as the exposure time increased from 10 to 300 s in 25, 50, and 75 ms on-time, respectively. However, the number of viable cells significantly decreased after the application of NBP for 600 s (Figure 2(a)). We found that the NBP treatment was not harmful to HGF viability up to 300 s at a low exposure time of NBP [Figure 2(b)].

Next, we evaluated the apoptosis of HGFs using the crystal violet stain after NBP treatment every 4 days. The HGFs made the colony units depending on the cultured time after 7 days. However, colony formation in the NBP-treated group was inhibited by cumulative air-plasma application on days 3, 7, and 11, as indicated by crystal violet staining [Figure 2(c)]. Quantification at 450 nm absorbance showed less colony formation [Figure 2(d)].

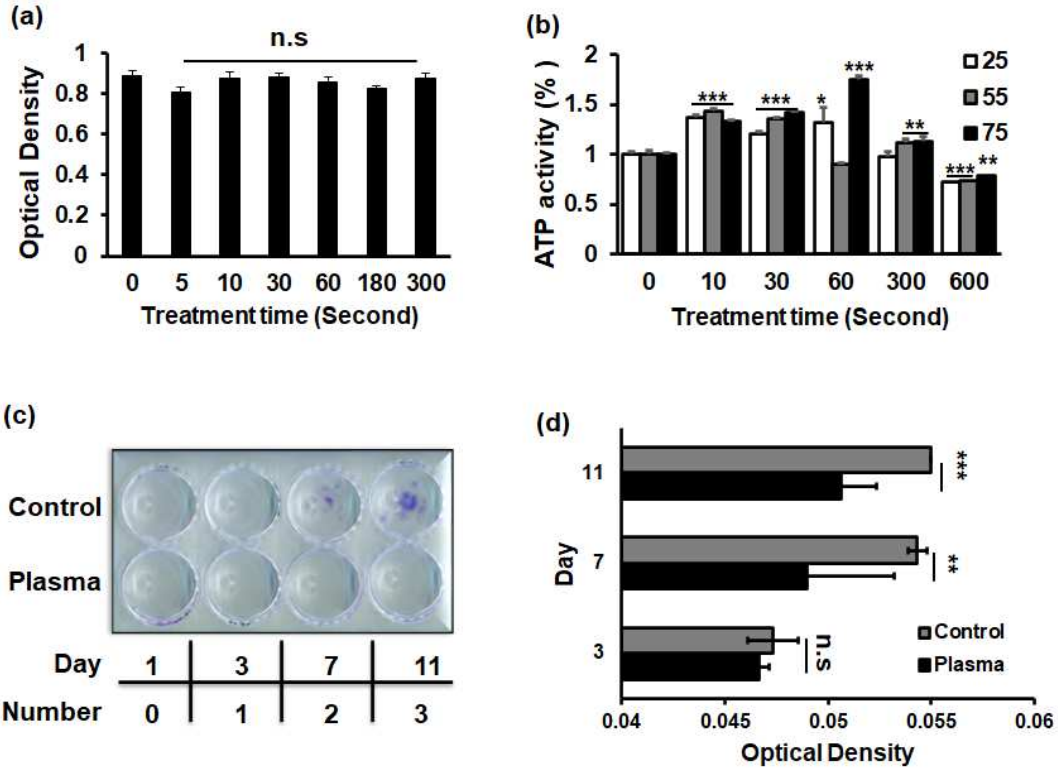

Figure 2. Effects of NBP on the viability and colony formation ability of human gingival fibroblasts (HGFs). (a) Cell viability was assessed using MTS reagent. Cells were seeded (1×10^2 per mm^2 area in common media) in 35mm dishes for growth analysis. The viability of HGFs was stable as the exposure time increased from 10 to 300 s in MTS assay. Data represent the mean without any significant differences among groups. (b) Validation of ATP levels after treatment with NBP using Cell-Titer-Glo. After counting the cells, cells were used to evaluate this relative ATP content by luminescence. The metabolic capacity of HGFs was slightly elevated or stable as the exposure time increased from 10 to 300 s in the ATP activity assay. However, the ATP

activity in cells decreased significantly after the application of NBP for 600 s in 25, 50, and 75 ms on-time (all *P*-value < 0.001). (c) Cumulative application of NBP inhibited colony formation in fibroblasts. The cells were stained with 0.5 % crystal violet, and colonies of more than 50 fibroblasts were counted. (d) Colony changes in incubation days for cell populations treated as in (c) (** p < 0.01, *** p < 0.001, t-test). Quantification at 450 nm absorbance also showed less staining in cells after NBP application at days 7 and 10. The bar graph shows the associated colony formation ability of NBP treatment compared with control cells.

3.4. Live/Dead assay to enumerate viable cells

Plasma treatment showed minimal toxicity to HGF cells. Cell viability was detected by using a live/dead assay kit (with 4 μM of EthD-1 and 2 μM of calcein AM) after plasma treatment for 3, 5, and 10 min (Figure 3). Moreover, to eliminate the working gas effect, we performed the only-gas treatment for 5 and 10 min in cells without plasma discharge.

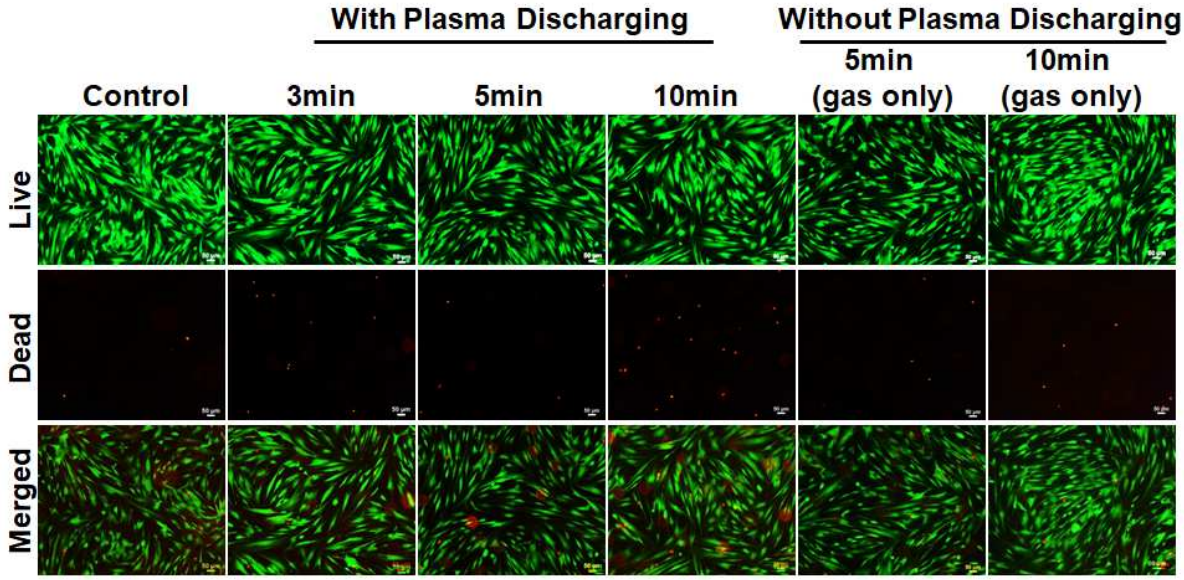

Figure 3. Plasma treatment showed minimal toxicity to HGF cells. Live and dead staining were evaluated by confocal analysis, and data were represented as fluorescence density. Cell toxicity after being treated with NBP was detected a by live/dead assay kit (with 4 μM of EthD-1 and 2 μM of calcein AM) with plasma treatment time for 3, 5, and 10 min. The working gas effect was eliminated by performing the only-gas treatment for 5 and 10 min in cells without plasma discharge. The green fluorescence indicates live cells, while red fluorescence indicates dead cells under the confocal microscope and then merged by Olympus FluoView software. The scale bar represents 50 μm. EthD-1, Ethidium homodimer I, calcein AM, calcein acetoxymethyl.

3.5. Increased migratory activity by NBP on HGFs

HGFs were assessed for migration activity after NBP treatment with the basal medium. We treated HGFs with NBP every day for 3 and 5 min and took a picture immediately after treatment. In migration assay, a peak increase in the migration of HGFs was noted on days 1, 2, and 3 following plasma application. HGFs treated with plasma for 3 min (2 L/min, 25 ms on-time, and 150 ms off-time) migrated towards each other across the gap faster than HGFs in the control and 5-min treatment groups (Figure 4).

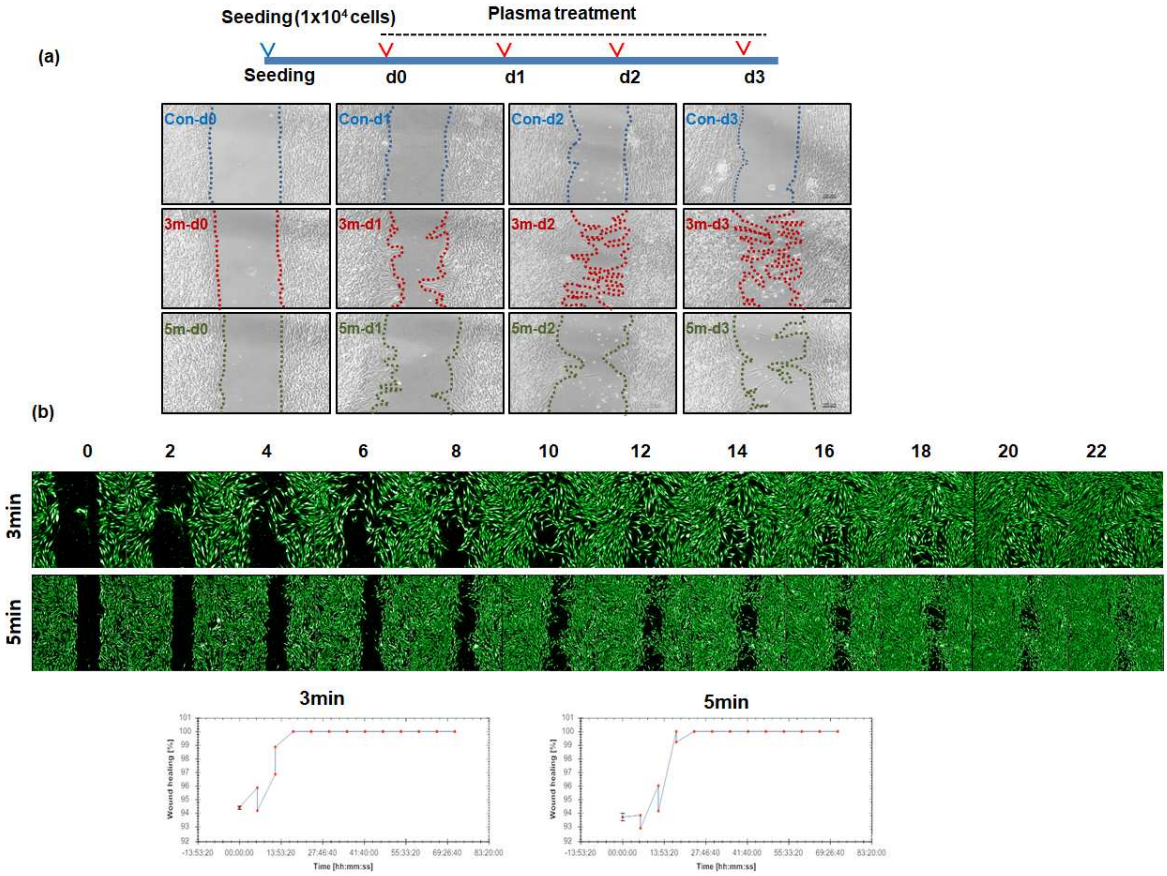

Figure 4. Effect of NBP on human gingival fibroblast (HGF) migration. (a) Scratch wound healing assay using HGF cells. Representative pictures of NBP-treated HGFs at 0, 3, and 5 min for three consecutive days. The wound closure assay pictures were taken every day. Air-plasma was applied for three consecutive days (25 ms on-time, 150 ms off-time, 2 L/min). The cells treated for 3 min migrated towards each other, compared to the cells in the control and 5-min treatment groups. Representative time-lapse images of monolayer cultures for HGFs after DBD-NBP treatment. (b) Scratch-wound closure was observed over time in HGFs by NBP treatment. Wound healing of HGFs was increased by bio-plasma treatment. HGFs treated with bio-plasma for 3 min closed 2 h earlier than those treated for 5 min, and the time to complete closure was 4 h faster. Wound closure is expressed as the remaining area uncovered by the cells.

3.6. Increased tissue remodeling by extracellular matrix (ECM) breakdown

The level of ECM breakdown was investigated. The metalloprotease (MMP) and pro-metalloprotease (pro-MMP) proteins were activated, indicating invigorated tissue remodeling. A zymography assay showed an increase in the activity of the MMP-9 complex, proMMP-2, and proMMP-9 proteins of plasma-treated HGFs, but not of the control HGFs [Figure 5(a)]. Next, differences in gene expression patterns of MMP-2 transcripts between the control and plasma-treated HGFs were evaluated. The latter showed significantly higher MMP-2 expression levels than the former [Figure 5(b)]. To determine whether ECM breakdown would affect the degradation of collagen structures, the gene expression patterns of types I or IV collagen and PDGF-β were investigated. No significant differences in the expression patterns of these genes were found between the control and plasma-treated groups (Figs. 5(c)–(e)).

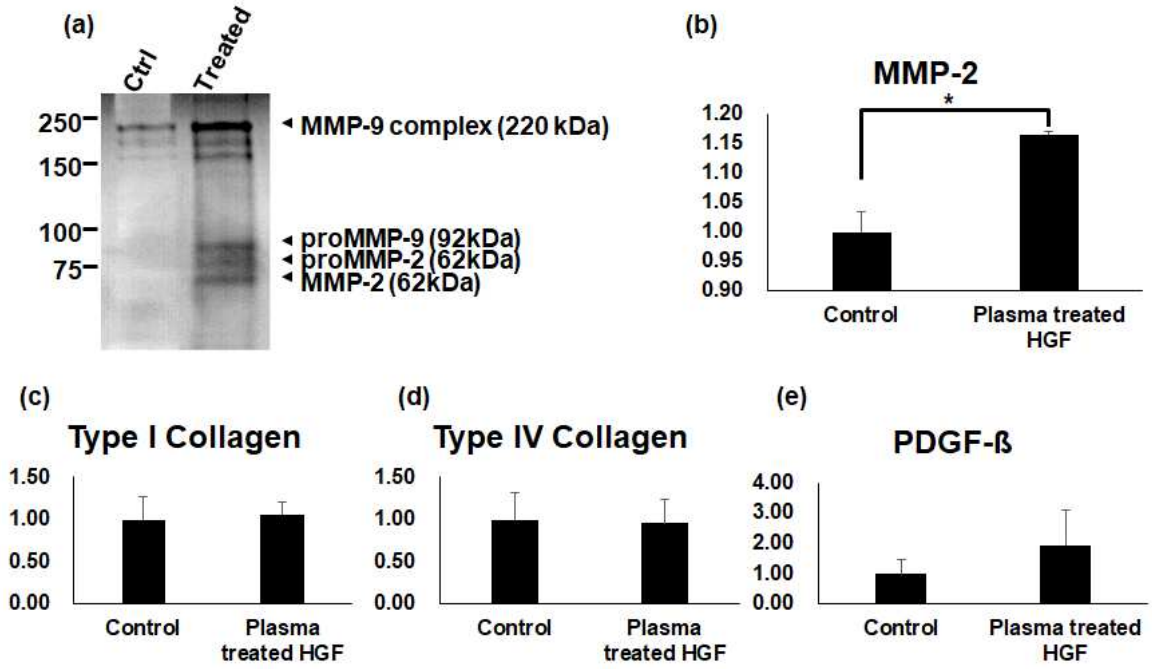

Figure 5. Extracellular matrix (ECM) destruction by non-thermal biocompatible plasma (NBP) on human gingival fibroblasts (HGFs). (a) Changes in proteinase activity were analysed by gelatinolytic zymography. Image were inverted (original blot is in supplementary information) (b) Relative amount of MMP2 transcript, (c) Transcripts of Type I collagen, (d) Transcript of Type IV collagen, and (e) PDGF-β (*P-value < 0.05). Full-length blots/gels are presented in the supplementary information file.

3.7. Induction of cell cycle arrest and cell migration

First, we investigated whether NBP affects cell cycle regulation by assessing the expression of the *p21* gene, which is related to cell cycle arrest. Consequently, a significant increase in *p21* expression was observed

in plasma-treated HGFs, compared to the control cells [Figure 6(a)]. Plasma-treated HGFs also showed elevated p21 protein levels, as indicated by immunoblot analysis (Figure 6(b)).

In migrating cells, there is a particular mechanism, involving not only cytoskeletal change but also a signaling pathway, to stimulate MMPs. The vascular endothelial growth factor (VEGF), protein kinase B (AKT)-mammalian target of rapamycin (mTOR), and focal adhesion kinase (FAK pathways were assessed after treatment with NBP for 3 min. The migration-related gene *VEGF* was expressed at significantly higher levels in plasma-treated HGFs than in control cells (Figure 6(c)). The activation of AKT-mTOR and p-FAK were also confirmed in NBP-treated HGFs by western blotting, which indicated that these downstream pathways were involved in cell migration (Figure 6(d), (e)). Finally, we evaluated the gene and protein expression levels of AKT and FAK and observed an increase in 3-min-treatment HGFs, but a slight decrease in 5-min-treatment HGFs (Figure 6(f), (g)). These results demonstrated that low-dose NBP treatment was effective for cell migration.

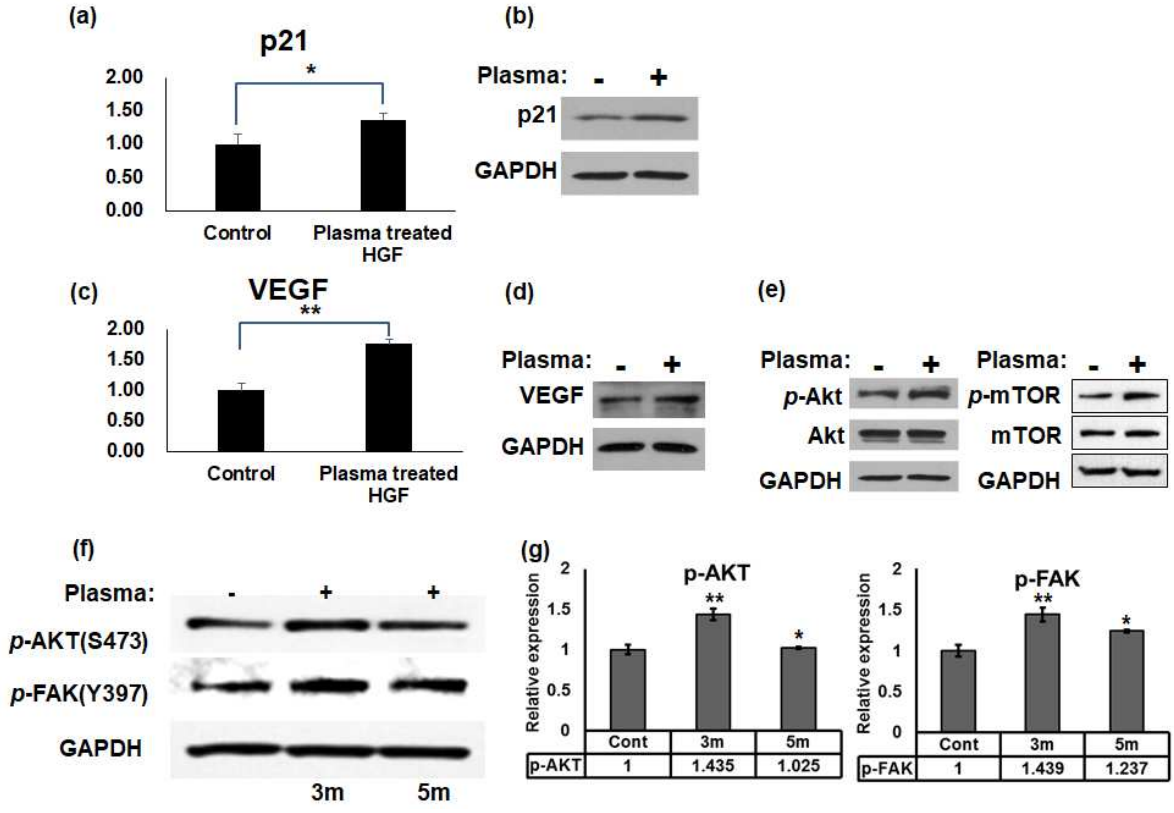

Figure 6. Induction of cell cycle arrest and cell migration. (a) Expression of the cell cycle arrest-related gene, *p21*. (b) The increased amount of p21 protein. (c) Increased expression of the angiogenesis-related gene *VEGF*. (d) Increased amount of VEGF protein. (e) Increased activity of AKT-mTOR signaling molecules induced by NBP. (f) Activity of AKT and FAK proteins at 3 and 5 min (**P*-value < 0.05, ***P*-value < 0.01). (g) Relative

expression levels of p-AKT and p-FAK. Full-length blots/gels are presented in the supplementary information file.

3.8. Plasma-stimulated cell migration through the FAK-related pathway

A wound healing assay was performed to evaluate the migration of HGF cells after treatment with 1) FAK inhibitor only, 2) NBP treatment for 3 min, and 3) FAK inhibitor combined with NBP treatment for 3 min compared with 4) control and observed up to 5 days [Fig 7(a)]. The treatment with NBP facilitated the gap closure in cells, whereas that with FAK inhibitor attenuated it. NBP application slightly reversed the activity of FAK inhibitor. HGF cells were stained with crystal violet at day 0 and day 3 [Fig 7(b)]. The percentage of the uncovered gap area in each representative image is shown as % of day 0 for each group (Fig 7(c)).

The cell movement is indicated by the actin filaments aligned in the shape. Migration speeds were strongly correlated with focal adhesion (FA) organization, where the cells with more aligned adhesions were considered to be migrating faster [36]. We have assessed the plasma treatment that rearranged the stress fibre of HGF cells. Plasma treatment enhanced the rearrangement of HGF cell's actin cytoskeleton, which facilitated cell migration. On the other hand, FAK inhibitor attenuated the plasma effect of actin cytoskeleton rearrangement and shortened actin fibres, indicating plasma-enhanced cell migration through the FAK-related cell signaling pathway (Fig 7(d)).

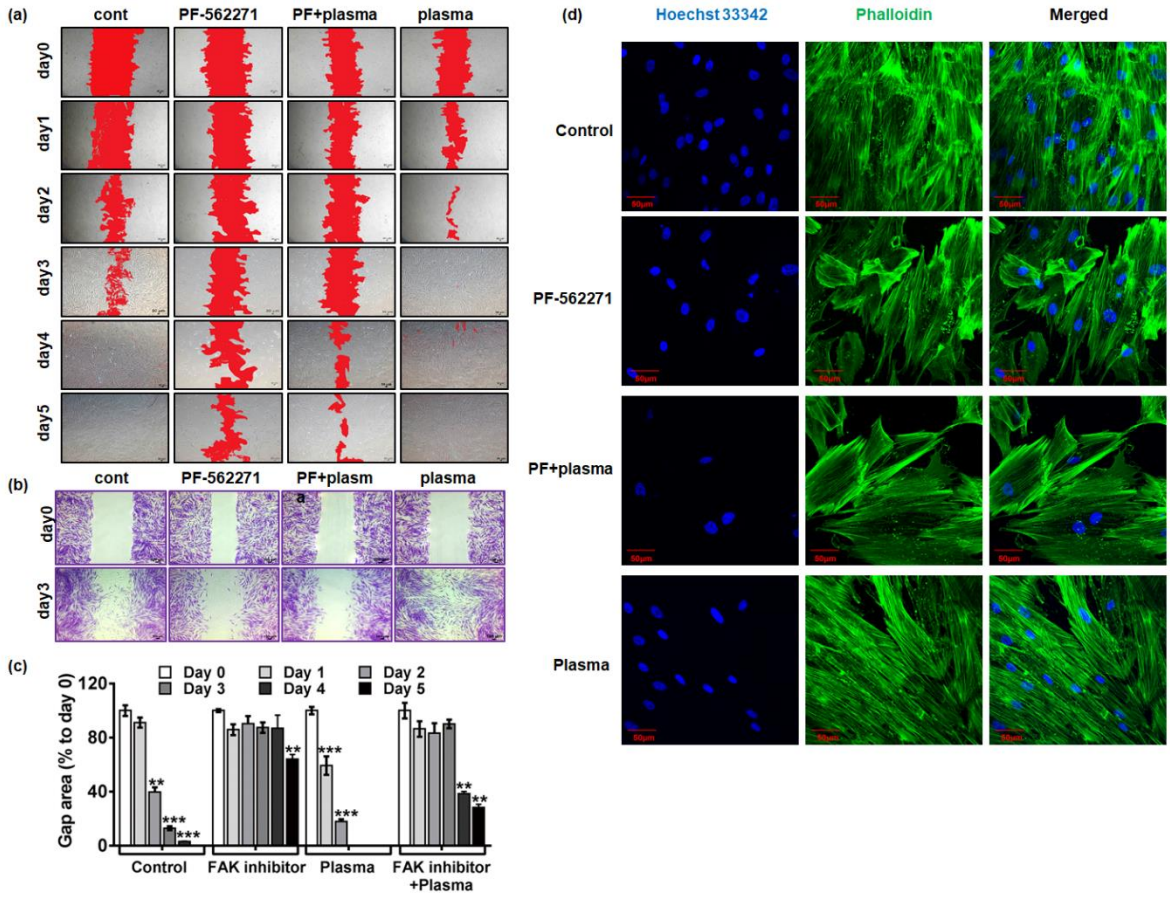

Figure 7. Plasma-stimulated cell migration through the FAK-related pathway. (a) A wound healing assay was performed to evaluate the migration of HGF cells after treatment with FAK inhibitor, plasma treatment for 3 min, and FAK inhibitor + plasma treatment for 3 min with observation for up to 5 days. The scale bar represents 50 μm. (b) The percentage of uncovered gap area in each representative image is shown as % of day 0 for each group. Data are represented as means ± SD obtained from three independent experiments. (**P*-value <0.05, ***P*-value < 0.01, ****P*-value < 0.001) (c) HGF cells were stained with crystal violet on day 0 and day 3, respectively. Scale bar represents 100 μm. FAK, focal adhesion kinase; HGF, human gingival fibroblast. Plasma treatment rearranged the stress fibre of HGF cells (d). Cells were treated with plasma for 3 min, with or without FAK inhibitor, and cultured for 72 h. Cells were identified by actin staining with Alexa Fluor 488-phalloidin (green) and nuclei were counterstained with Hoechst 33342 (blue). Plasma treatment enhanced actin cytoskeleton rearrangement in HGF cells, which facilitated cell migration. On the other hand, the FAK inhibitor attenuated the plasma effect on actin cytoskeleton rearrangement and shortened actin fibers, indicating plasma-enhanced cell migration through the FAK-related cell signaling pathway. Scale bar = 50 μm.

3.9. Effect of oxidation on the stability and conformation of the FAK protein

In section 2.6., we demonstrated by protein expression experiments a clear activation of the FAK protein at 3 min (low dose) of plasma exposure [Figure 6(f), (g)], which coincided with the results of the cell migration experiment (Figure 7). To support these experiments and to study the effect of FAK oxidation at the atomic level, we performed molecular dynamics (MD) simulations. Specifically, we focused on the catalytic domain of the FAK protein, i.e. the kinase domain (KD), which is mainly responsible for initiating the kinase signaling cascade [37]. Any modification in the KD (e.g. mutation or oxidation of its residues) can lead to the disruption of its interaction with the FERM (Four-point-one, ezrin, radixin, moesin) domain, which results in the phosphorylation of Tyr397 (as observed in Figure 6(f)), eventually leading to the full catalytic activation of the enzyme [38,39].

To understand the effect of plasma oxidation on the KD of FAK, we oxidised specific amino acids (AAs), based on their chemical reactivity and modification, as well as their solvent accessible surface areas (SASAs) calculated in our simulations. Thus, we oxidised six KD residues (i.e. Cys427, Met442, Cys559, Met571, Met617, and Met643) that are highly reactive and have higher accessibility to solvent (see Table S1 in the Supplementary Information). To oxidise these AAs, we modified the Cys residues to cysteic acid moieties and the Met residues to methionine sulfoxides (see Table S2 in the Supplementary Information) based on [30,31].

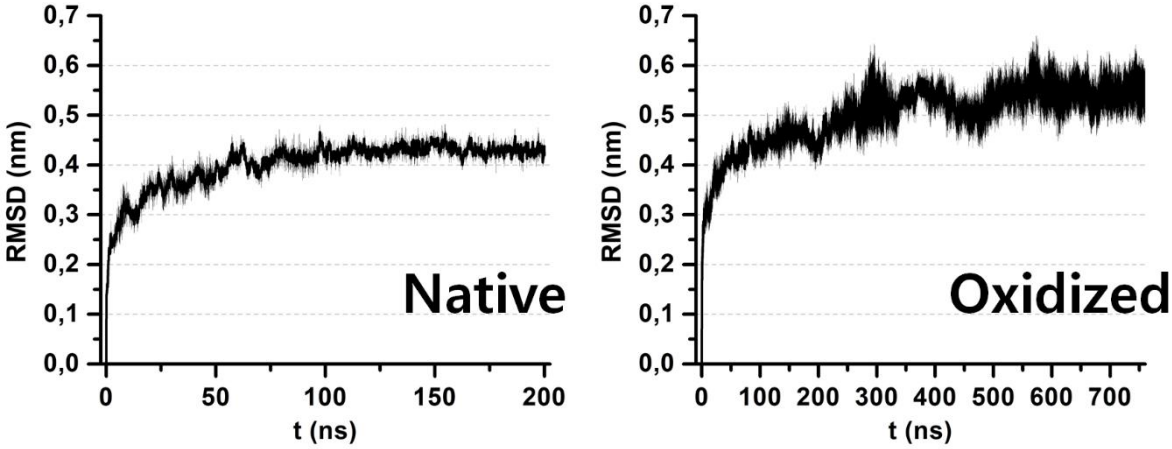

Figure 8. Computer simulation. Average root means square deviations (RMSDs) of the alpha carbons of the native and oxidised kinase domains (KDs) of FAK.

Figure 8 illustrates the time evolution of the root mean square deviations (RMSDs) of the alpha carbons of the native and oxidised KDs, averaged over three simulations for each protein system.

It is clear that the native KD equilibrates after 100 ns and remains stable during the rest of the simulation time, yielding an RMSD fluctuating around 0.43 nm. In contrast, the oxidised KD stabilises only at around 500 ns, at a higher RMSD value, fluctuating around 0.55 nm. Thus, oxidation leads to higher fluctuations of the RMSD, indicating that the oxidised KD becomes slightly more flexible. This is due to the conformational changes in the protein domain. Indeed, the results of the secondary structure analysis show slight alterations in the secondary structure of the KD after oxidation. Upon oxidation, the percentage of the random coil structure in the KD increases and the α-helix structure decreases by approximately 2–3 %, whereas other conformations stay more or less unchanged (see Table S3 in the Supplementary Information). Thus, oxidation results in a slight increase in structural flexibility, thereby affecting protein stability. Note that the oxidation degree used in our simulations was low, which corresponded to the short plasma treatment time (3 min) used in our experiments. Therefore, it does not lead to drastic conformational changes. However, it is most likely sufficient to change the function of the FAK protein and thus affect its catalytic activity.

4. Discussion

This study determined that NBP accelerated the migration of HGFs. The migratory effect could be supported by new vessel formation and ECM breakdown. Overall, these synergistic actions of NBP could establish favourable wound beds and result in enhanced wound healing.

Favourable wound healing by NBP has been reported in several *in vivo* rodent studies [40,41]. Enhanced wound repair enabled more elastic tissue retention, because of less tissue damage, and allowed less leukocyte production, because of bacterial load reduction [42]. The healing of pruritic and necrotic leg wounds of patients has been proven to be clinically efficient and reliable [43,44]. Accelerated re-epithelialisation, fewer fibrin layers and blood crusts, and normal wound surroundings have also been found on the skin donor sites of 34 patients after NBP application [45].

The present study found that low-dose NBP treatment did not inhibit HGF proliferation. Moreover, previous studies showed that low-dose NBP treatment did not suppress the proliferation or viability of keratinocytes [12,46,47], fibroblasts [48], endothelial cells [49], or immune cells [50]. Using a plasma device with surface microdischarge technology, one study using the gamma-H2AX stain assay reported that plasma application for up to 2 min was endurable to the *ex vivo* human skin samples without DNA damage, although toxic products, such as ozone, NO, and UV, were discharged [51].

This study showed elevated p21 levels in plasma-treated HGFs. The *p21* gene, also known as cyclin-dependent kinase inhibitor 1, is a potent cell cycle regulator from phase G1 to S [52]. It is involved in cell senescence as well as growth cessation. Several previous studies have shown the regulatory role of NBP on DNA. In a study using keratinocytes, the G2/M phase arrest of the cells was found after NBP application [53], and cell cycle arrest was dependent on plasma sources and application time [12,23]. An experiment of human keratinocytes revealed the time-dependent loss of viable cells and linear increase in DNA damage after 24 h of NBP application [12], reporting an increased number of G2/M phase cells and decreased number of G1 phase cells. This phenomenon has been also found in other studies with cancer cells, indicating that G2/M phase arrest is a common pathway after NBP application [23].

Increased response of the matrix metalloproteinases (MMPs)-2, and -9 is an important finding of this study. The extracellular matrix is remodeled by matrix metalloproteinases (MMPs). Neutrophils, microglia, and endothelial cells all produce gelatinase B (MMP-9) which is an inducible 92 kDa MMP. Gelatinase A (MMP-2) is a 72-kDa MMP that is found in abundance in the brain. MMP activity has been associated with a variety of pathologic disorders, and MMP inhibitors are being studied in a few experimental models for their therapeutic usefulness. The proMMP-2 and -9 and MMP-9 complex were more highly activated in the plasma-treated group than in the control group. Furthermore, a relative gene expression profile showed that MMP-2 was expressed at higher levels in the plasma-treated group than in the control group. Tissue inhibitors of metalloproteinases (TIMPs) control MMP activity, which is essential for ECM homeostasis. TIMPs are well-known for their ability to reduce MMP activity and thus prevent tumour development and metastasis. TIMPs have the ability to bind to all known MMPs and inhibit their activity by forming noncovalent complexes with them. As a result, TIMPs play an important role in balancing the delicate balance of ECM breakdown and reconstruction. MMP acts as a protease to decompose structural components of the ECM, creating space for cells to migrate, allowing tissue remodeling, and enabling signal transduction [54]. Meanwhile, this study could not show differences in type I and IV collagen gene expression between the control and plasma-treated groups. This was in contrast to the previous report on the positive role of NBP on human dermal fibroblasts, which promoted the production of type I collagen [55]. Further studies are required to determine the accurate role of NBP in collagen breakdown.

This study found the elevation of the AKT activity and *VEGF* gene expression. One study demonstrated that AKT plays a key role in endothelial cell signal transduction that induces migration and is required for VEGF to stimulate cell migration [56,57]. The serine/threonine kinase AKT is a key signaling molecule for functional regulation, including cell survival and growth. It also plays an important role in cell motility, such as tumor invasion, by actin cytoskeleton modification [58] or via MMP-9 production [59].

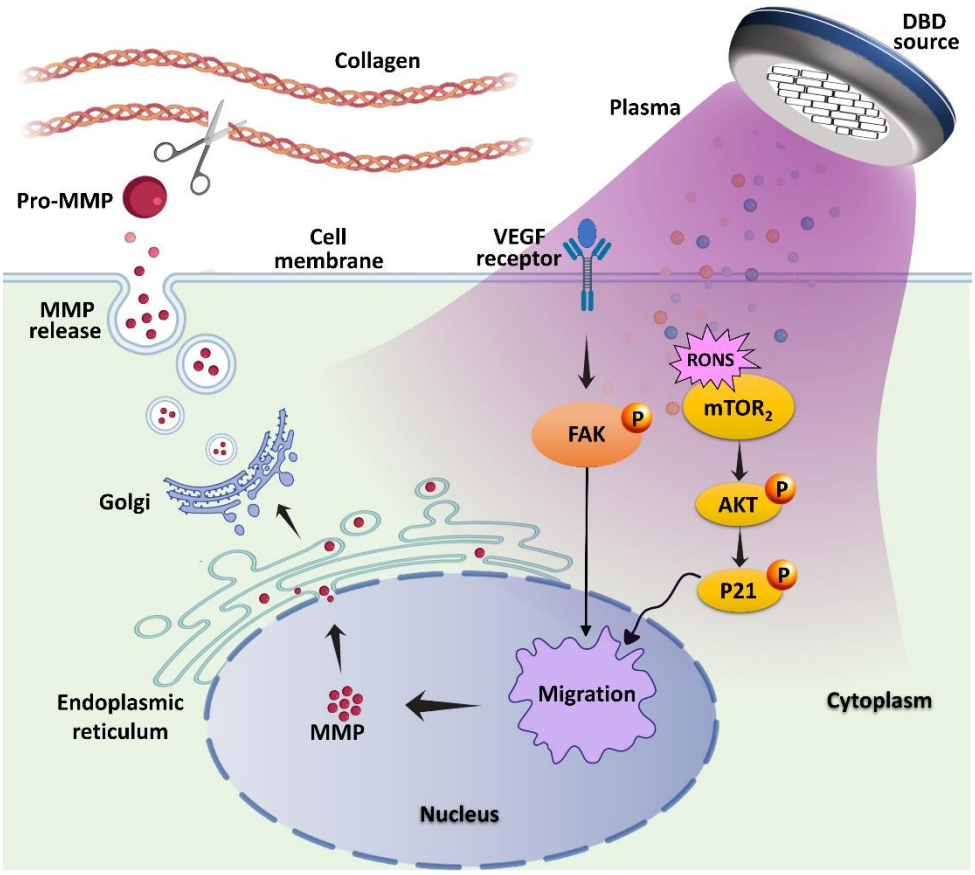

Figure 9. Low dose non-thermal biocompatible dielectric barrier discharge plasma increases the motility and reparative properties of human gingival fibroblasts. NBP stimulates the migration of human HGF cells by enhancing PI3K/AKT pathways that can affect the p21 signals and promotes the production and secretion of MMPs through FAK expression regulation.

Previously, an important role of the AKT-mTOR pathway in wound healing was suggested. One report showed that AKT-mTOR activation could elevate epithelial cell migration and wound healing in the mouse model [60]. Another report revealed that the dysfunction of AKT-mTOR signalling pathway resulted in impaired wound healing in diabetic rats [60]. The present study also supported the above pathway; therefore, NBP application could have an important role in the activation of mucosal healing.

We also observed the peak activation patterns of both AKT and FAK molecules at 3 min of plasma exposure, which coincided with the cell migration results. Attenuation of cell migration or actin cytoskeleton rearrangement by FAK inhibitor but reversal by NBP indicated that NBP enhanced cell migration through the FAK-related cell signaling pathway. One report showed that the activation of VEGF receptor leads to the activation of downstream FAK and phosphoinositide 3-kinase (PI3K)/AKT [61,62]. Another study demonstrated

that phosphorylated FAK was responsible for angiogenesis [63]. Therefore, low-dose DBD-NBP could accelerate cell migration via upregulating p-AKT and p-FAK (Tyr 397), and VEGF proteins.

Collectively, the supposed hypothesis for the mechanism of HGF migration is that three steps are involved in the migration of the HGFs. The first step is cell cycle arrest. The low-dose plasma may stop the cell cycle but is not lethal to cells. The second step is ECM disruption for the establishment of the migrating bed for easier transportation of cells. Finally, HGF migration occurs as a result of the outward migrating signal cascade. Wound closure time is different compared to the cells and actual animals. Just for the cell, wound closure was finished for several days less than a week according to cell numbers and wound distance which we made. To avoid this issue, we use iBidi system the width of cell free gap is 500 µm +/- 100 µm. In this case, the wound closure was finished until 3 days on average time. After all, we observed significant results between groups compared with the control, plasma treated group shows more fast closure end even 3 min and 5 min. between 3 min and 5 min, 3 min plasm treated group is better ability than 5 min plasma treated group for wound closure. The HGFs detach and move to the middle of the wound until the wound closure is completed. As it is known that MMPs action or ECM breakdown alone cannot guarantee cellular migration, VEGF-AKT-FAK- or AKT-mTOR-related signal transduction would aid the migration process.

The FAK protein plays an important role in cell-cell and cell-matrix interaction and is a promising drug target. It is composed of an FERM domain and a catalytic KD that controls its enzymatic activity. FAK maintains its auto-inhibited conformation by a strong interaction between its FERM domain and KD, and during this auto-inhibited state, it protects its activation loop from phosphorylation by Src kinase. Disruption of the FERM-KD interaction leads to the auto-phosphorylation of Tyr397 (situated in the FERM-KD linker), resulting in full catalytic activation of the FAK protein [38,39,64].

A few studies demonstrated that ROS induces tyrosine phosphorylation of FAK through a variety of cellular signaling pathways [65,66]. However, none of them explained the cause of FAK activation or discussed the oxidation-related changes in the conformation of this protein at the atomic level. In our MD simulations, we showed that the oxidation of its KD, the degree of which most likely corresponds to a short plasma treatment time (3 min), resulted in a higher RMSD value (Figure 8). This indicates that the oxidised KD is slightly more flexible than the native KD, which is because of the conformational changes in the protein. Thus, oxidation induces a slight increase in the structural flexibility of KD, thus affecting its stability. This in turn might disrupt the FERM-KD interaction, leading to the phosphorylation of its Tyr397 residue [as observed in Figure 6(f)] and ultimately to an increase in its catalytic activity. The latter can be correlated with the expression of the FAK

protein observed in Figure 6(g). Thus, our simulation results are qualitatively in line with our experimental results.

In our experiments, we observed a decrease in the FAK protein expression at a higher oxidation dose (i.e. 5 min of plasma treatment) compared to a lower oxidation dose (i.e. 3 min of plasma exposure). A decrease in FAK expression may be associated with an increase in the FERM-KD interaction. A longer (5 min) plasma exposure leads to a high probability of the oxidation of other AAs, such as Trp, Phe, Tyr, or His, which are also vulnerable to oxidation after Met and Cys [30] and are present in the KD of the FAK protein. The plasma-induced oxidation of Trp, Phe, Tyr, and His mainly results in the hyrdroxylation of these AAs [30,31]. This might subsequently increase the hydrophilic interaction of these AAs with other AAs in the FERM domain, by the formation of hydrogen bonds, which can again restore the FERM-KD interaction. This can then result in the hypo-phosphorylation of the FAK protein [67], leading to a reduction of its catalytic activity. Nevertheless, as shown in [Figure 6(f), (g)], the FERM-KD interaction is the strongest in the native FAK protein, both after high- (5 min) and low-dose (3 min) plasma treatments.

This study analysed the effect of DBD-NBP on HGFs, and to the best of our knowledge, this is the first study to elucidate the signaling pathway underlying the migratory effect of NBP. Furthermore, this study elucidated the role of DBD-NBP in migration-related actin cytoskeleton modification.

In conclusion, low-dose DBD-NBP induced cell cycle arrest, ECM breakdown, and subsequent migration in host cells. Our simulation results revealed that the plasma-induced oxidation of the KD of the FAK protein (i.e. chemical modifications in its residues) leads to instability and conformational changes in the protein. This can lead to a disruption of the FERM-KD interaction, eventually resulting in an increase in the catalytic activity of the FAK enzyme. Hence, our simulation results are qualitatively in line with our experimental observations. These consecutive reactions would be beneficial for a fast and enhanced wound healing process. Thus, non-thermal DBD plasma could be used as a promising tool for enhanced wound healing.

References

[1] K. P. Arjunan, V. K. Sharma, S. Ptasinska, *Int. J. Mol. Sci.* **2015**, *16*, DOI 10.3390/ijms16022971.

[2] S. Hasse, T. Duong Tran, O. Hahn, S. Kindler, H. R. Metelmann, T. Von Woedtke, K. Masur, *Clin. Exp. Dermatol.* **2016**, *41*, DOI 10.1111/ced.12735.

[3] G. E. Morfill, T. Shimizu, B. Steffes, H. U. Schmidt, *New J. Phys.* **2009**, *11*, DOI 10.1088/1367-2630/11/11/115019.

[4] T. Maisch, T. Shimizu, G. Isbary, J. Heinlin, S. Karrer, T. G. Klämpfl, Y. F. Li, G. Morfill, J. L. Zimmermann, *Appl.*

Environ. Microbiol. **2012**, *78*, DOI 10.1128/AEM.07235-11.

[5] J. L. Zimmermann, K. Dumler, T. Shimizu, G. E. Morfill, A. Wolf, V. Boxhammer, J. Schlegel, B. Gansbacher, M. Anton, *J. Phys. D. Appl. Phys.* **2011**, *44*, DOI 10.1088/0022-3727/44/50/505201.

[6] M. Hähnel, T. Von Woedtke, K. D. Weltmann, *Plasma Process. Polym.* **2010**, *7*, DOI 10.1002/ppap.200900076.

[7] S. Mumtaz, J. N. Rana, E. H. Choi, I. Han, *Int. J. Mol. Sci.* **2022**, *23*, DOI 10.3390/ijms23169288.

[8] G. Isbary, T. Shimizu, Y. F. Li, W. Stolz, H. M. Thomas, G. E. Morfill, J. L. Zimmermann, *Expert Rev. Med. Devices* **2013**, *10*, DOI 10.1586/erd.13.4.

[9] E. D. Yildirim, H. Ayan, V. N. Vasilets, A. Fridman, S. Guceri, W. Sun, *Plasma Process. Polym.* **2008**, *5*, DOI 10.1002/ppap.200700041.

[10] Y. T. Chang, G. Chen, *J. Dent. Sci.* **2016**, *11*, DOI 10.1016/j.jds.2014.03.007.

[11] P. Sun, J. Pan, Y. Tian, N. Bai, H. Wu, L. Wang, C. Yu, J. Zhang, W. Zhu, K. H. Becker, et al., in *IEEE Trans. Plasma Sci.*, **2010**.

[12] S. Blackert, B. Haertel, K. Wende, T. von Woedtke, U. Lindequist, *J. Dermatol. Sci.* **2013**, *70*, DOI 10.1016/j.jdermsci.2013.01.012.

[13] A. Barzilai, K. I. Yamamoto, *DNA Repair (Amst).* **2004**, *3*, DOI 10.1016/j.dnarep.2004.03.002.

[14] Y. S. Bae, H. Oh, S. G. Rhee, Y. Do Yoo, *Mol. Cells* **2011**, *32*, DOI 10.1007/s10059-011-0276-3.

[15] I. B. Slimen, T. Najar, A. Ghram, H. Dabbebi, M. Ben Mrad, M. Abdrabbah, *Int. J. Hyperth.* **2014**, *30*, DOI 10.3109/02656736.2014.971446.

[16] P. Sestili, C. Fimognari, *Biomed Res. Int.* **2015**, *2015*, DOI 10.1155/2015/402386.

[17] J. Balzer, K. Heuer, E. Demir, M. A. Hoffmanns, S. Baldus, P. C. Fuchs, P. Awakowicz, C. V. Suschek, C. OplÃnder, *PLoS One* **2015**, *10*, DOI 10.1371/journal.pone.0144968.

[18] M. Laroussi, *Plasma Process. Polym.* **2005**, *2*, DOI 10.1002/ppap.200400078.

[19] D. B. Graves, *J. Phys. D. Appl. Phys.* **2012**, *45*, DOI 10.1088/0022-3727/45/26/263001.

[20] K. P. Arjunan, G. Friedman, A. Fridman, A. M. Clyne, *J. R. Soc. Interface* **2012**, *9*, DOI 10.1098/rsif.2011.0220.

[21] U. Kogelschatz, *Plasma Chem. Plasma Process.* **2003**, *23*, DOI 10.1023/A:1022470901385.

[22] G. Isbary, J. L. Zimmermann, T. Shimizu, Y. F. Li, G. E. Morfill, H. M. Thomas, B. Steffes, J. Heinlin, S. Karrer, W. Stolz, *Clin. Plasma Med.* **2013**, *1*, DOI 10.1016/j.cpme.2012.11.001.

[23] B. Haertel, T. von Woedtke, K. D. Weltmann, U. Lindequist, *Biomol. Ther.* **2014**, *22*, DOI 10.4062/biomolther.2014.105.

[24] K. J. Baek, Y. Choi, S. Ji, *Arch. Oral Biol.* **2013**, *58*, DOI 10.1016/j.archoralbio.2013.07.007.

[25] I. Han, S.-J. Jeong, H.-J. Lee, W. Koh, H.-J. Lee, E.-O. Lee, H. S. Kim, S. J. Lee, C.-Y. Chen, M.-H. Jung, et al., *Proteomics* **2011**, *11*, DOI 10.1002/pmic.201000475.

[26] T. Gebäck, M. M. P. Schulz, P. Koumoutsakos, M. Detmar, *Biotechniques* **2009**, *46*, DOI 10.2144/000113083.

[27] G. Bussi, D. Donadio, M. Parrinello, *J. Chem. Phys.* **2007**, *126*, DOI 10.1063/1.2408420.

[28] M. Parrinello, A. Rahman, *J. Appl. Phys.* **1981**, *52*, DOI 10.1063/1.328693.

[29] I. G. Tironi, R. Sperb, P. E. Smith, W. F. Van Gunsteren, *J. Chem. Phys.* **1995**, *102*, DOI 10.1063/1.469273.

[30] E. Takai, T. Kitamura, J. Kuwabara, S. Ikawa, S. Yoshizawa, K. Shiraki, H. Kawasaki, R. Arakawa, K. Kitano, *J. Phys. D. Appl. Phys.* **2014**, *47*, DOI 10.1088/0022-3727/47/28/285403.

[31] R. Zhou, R. Zhou, J. Zhuang, Z. Zong, X. Zhang, D. Liu, K. Bazaka, K. Ostrikov, *PLoS One* **2016**, *11*, DOI 10.1371/journal.pone.0155584.

[32] M. J. Abraham, T. Murtola, R. Schulz, S. Páll, J. C. Smith, B. Hess, E. Lindah, *SoftwareX* **2015**, *1–2*, DOI 10.1016/j.softx.2015.06.001.

[33] N. Schmid, A. P. Eichenberger, A. Choutko, S. Riniker, M. Winger, A. E. Mark, W. F. Van Gunsteren, *Eur. Biophys. J.* **2011**, *40*, DOI 10.1007/s00249-011-0700-9.

[34] D. Petrov, C. Margreitter, M. Grandits, C. Oostenbrink, B. Zagrovic, *PLoS Comput. Biol.* **2013**, *9*, DOI 10.1371/journal.pcbi.1003154.

[35] I. Han, E. H. Choi, *Oncotarget* **2017**, *8*, DOI 10.18632/oncotarget.16821.

[36] W. Y. Wang, A. T. Pearson, M. L. Kutys, C. K. Choi, M. A. Wozniak, B. M. Baker, C. S. Chen, *APL Bioeng.* **2018**, *2*, DOI 10.1063/1.5052239.

[37] S. Abbi, H. Ueda, C. Zheng, L. A. Cooper, J. Zhao, R. Christopher, J. L. Guan, *Mol. Biol. Cell* **2002**, *13*, DOI 10.1091/mbc.E02-05-0295.

[38] D. Lietha, X. Cai, D. F. J. Ceccarelli, Y. Li, M. D. Schaller, M. J. Eck, *Cell* **2007**, *129*, DOI 10.1016/j.cell.2007.05.041.

[39] M. B. Calalb, T. R. Polte, S. K. Hanks, *Mol. Cell. Biol.* **1995**, *15*, DOI 10.1128/mcb.15.2.954.

[40] E. Stoffels, A. J. Flikweert, W. W. Stoffels, G. M. W. Kroesen, *Plasma Sources Sci. Technol.* **2002**, *11*, DOI 10.1088/0963-0252/11/4/304.

[41] E. García-Alcantara, R. López-Callejas, P. R. Morales-Ramírez, R. Peña-Eguiluz, R. Fajardo-Muñoz, A. Mercado-Cabrera, S. R. Barocio, R. Valencia-Alvarado, B. G. Rodríguez-Méndez, A. E. Muñoz-Castro, et al., *Arch. Med.*

Res. **2013**, *44*, DOI 10.1016/j.arcmed.2013.02.001.

[42] S. Salehi, A. Shokri, M. R. Khani, M. Bigdeli, B. Shokri, *Biointerphases* **2015**, *10*, DOI 10.1116/1.4914377.

[43] J. Heinlin, G. Isbary, W. Stolz, G. Morfill, M. Landthaler, T. Shimizu, B. Steffes, T. Nosenko, J. L. Zimmermann, S. Karrer, *J. Eur. Acad. Dermatology Venereol.* **2011**, *25*, DOI 10.1111/j.1468-3083.2010.03702.x.

[44] M. A. Bogle, K. A. Arndt, J. S. Dover, *Arch. Dermatol.* **2007**, *143*, DOI 10.1001/archderm.143.2.168.

[45] J. Heinlin, J. L. Zimmermann, F. Zeman, W. Bunk, G. Isbary, M. Landthaler, T. Maisch, R. Monetti, G. Morfill, T. Shimizu, et al., in *Wound Repair Regen.*, **2013**.

[46] B. Haertel, S. Straßenburg, K. Oehmigen, K. Wende, T. Von Woedtke, U. Lindequist, *Biomed Res. Int.* **2013**, *2013*, DOI 10.1155/2013/761451.

[47] B. Haertel, K. Wende, T. Von Woedtke, K. D. Weltmann, U. Lindequist, *Exp. Dermatol.* **2011**, *20*, DOI 10.1111/j.1600-0625.2010.01159.x.

[48] B. B. Lopes, M. B. De Paula Leite Kraft, J. Rehder, F. R. X. Batista, M. B. Puzzi, in *Procedia Eng.*, **2013**.

[49] S. Kalghatgi, G. Friedman, A. Fridman, A. M. Clyne, in *Ann. Biomed. Eng.*, **2010**.

[50] X. M. Shi, G. J. Zhang, Y. K. Yuan, Y. Ma, G. M. Xu, Y. Yang, *Plasma Process. Polym.* **2008**, *5*, DOI 10.1002/ppap.200700174.

[51] G. Isbary, J. Köritzer, A. Mitra, Y. F. Li, T. Shimizu, J. Schroeder, J. Schlegel, G. E. Morfill, W. Stolz, J. L. Zimmermann, *Clin. Plasma Med.* **2013**, *1*, DOI 10.1016/j.cpme.2012.10.001.

[52] A. L. Gartel, S. K. Radhakrishnan, *Cancer Res.* **2005**, *65*, DOI 10.1158/0008-5472.CAN-04-3995.

[53] O. Volotskova, T. S. Hawley, M. A. Stepp, M. Keidar, *Sci. Rep.* **2012**, *2*, DOI 10.1038/srep00636.

[54] A. Page-McCaw, A. J. Ewald, Z. Werb, *Nat. Rev. Mol. Cell Biol.* **2007**, *8*, DOI 10.1038/nrm2125.

[55] S. Arndt, P. Unger, E. Wacker, T. Shimizu, J. Heinlin, Y. F. Li, H. M. Thomas, G. E. Morfill, J. L. Zimmermann, A. K. Bosserhoff, et al., *PLoS One* **2013**, *8*, DOI 10.1371/journal.pone.0079325.

[56] M. Morales-Ruiz, D. Fulton, G. Sowa, L. R. Languino, Y. Fujio, K. Walsh, W. C. Sessa, *Circ. Res.* **2000**, *86*, DOI 10.1161/01.RES.86.8.892.

[57] R. Castilho, C. Squarize, J. Gutkind, *Oral Dis.* **2013**, *19*, DOI 10.1111/odi.12070.

[58] G. Xue, B. A. Hemmings, *J. Natl. Cancer Inst.* **2013**, *105*, DOI 10.1093/jnci/djs648.

[59] D. Kim, S. Kim, H. Koh, S. Yoon, T. Akt, B. Pkb, *FASEB J.* **2016**, *15*.

[60] C. H. Squarize, R. M. Castilho, T. H. Bugge, J. S. Gutkind, *PLoS One* **2010**, *5*, DOI 10.1371/journal.pone.0010643.

[61] B. J. Pyun, S. Choi, Y. Lee, T. W. Kim, J. K. Min, Y. Kim, B. D. Kim, J. H. Kim, T. Y. Kim, Y. M. Kim, et al.,

Cancer Res. **2008**, *68*, DOI 10.1158/0008-5472.CAN-07-2799.

[62] X. Wang, X. Fu, S. Zhao, X. Fu, H. Zhang, L. Shao, G. Li, C. Fan, *Mol. Med. Rep.* **2017**, *16*, DOI 10.3892/mmr.2017.7730.

[63] B. Tavora, S. Batista, L. E. Reynolds, S. Jadeja, S. Robinson, V. Kostourou, I. Hart, M. Fruttiger, M. Parsons, K. M. Hodivala-Dilke, *EMBO Mol. Med.* **2010**, *2*, DOI 10.1002/emmm.201000106.

[64] U. Grädler, J. Bomke, D. Musil, V. Dresing, M. Lehmann, G. Hölzemann, H. Greiner, C. Esdar, M. Krier, T. Heinrich, *Bioorganic Med. Chem. Lett.* **2013**, *23*, DOI 10.1016/j.bmcl.2013.07.050.

[65] S. Vepa, W. M. Scribner, N. L. Parinandi, D. English, J. G. N. Garcia, V. Natarajan, *Am. J. Physiol. - Lung Cell. Mol. Physiol.* **1999**, *277*, DOI 10.1152/ajplung.1999.277.1.l150.

[66] M. H. B. Mahdi, V. Andrieu, C. Pasquier, *IUBMB Life* **2000**, *50*, DOI 10.1080/15216540051081038.

[67] L. A. Cohen, J. L. Guan, *J. Biol. Chem.* **2005**, *280*, DOI 10.1074/jbc.M412021200.

Acknowledgements: T Acknowledgments: The authors would like to thank to Mr. Sang Hak Lee for providing device and his technical support for nonthermal plasma device used for this study.

Funding: This study was supported by the Basic Science Research Program through the National Research Foundation of Korea (NRF) funded by the Ministry of Education (grant number 2020R1I1A1A01073071 to Ihn Han and grant number 2021R1A6A1A03038785 to Ihn Han and Eun Ha Choi). The authors acknowledge the Core Laboratory for Convergent Translational Research in the College of Medicine, Korea University, for their technical support. The computational work was financially supported by the Research Foundation – Flanders (FWO) [grant number 1200219N].

The authors acknowledge the Turing HPC infrastructure at the CalcUA Core Facility of the University of Antwerp (UA), a division of the Flemish Supercomputer Center VSC, funded by the Hercules Foundation, the Flemish Government (department EWI) and the UA, where all computational work was performed.

Author information

Affiliations

Plasma Bioscience Research Center, Applied Plasma Medicine Center, Kwangwoon University, Seoul, 01897, Republic of Korea, Department of Plasma Bio-Display, Kwangwoon University, Seoul 01897, Korea

Ihn Han

Department of Dentistry, Korea University Anam Hospital, Seoul, 02841, Republic of Korea

In-Seok Song

Division of Pediatric Neurosurgery, Pediatric Clinical Neuroscience Center, Seoul National University Children's Hospital, Seoul, 03080, Republic of Korea.

Seung Ah Choi

Confocal Core Facility, Center for Medical Innovation, Seoul National University Hospital, Seoul 03082, Korea

Taebok Lee

Research group PLASMANT, Department of Chemistry, University of Antwerp, Universiteitsplein 1, B-2610 Antwerp, Belgium

Maksudbek Yusupov

Research group PLASMANT, Department of Chemistry, University of Antwerp, Universiteitsplein 1, B-2610 Antwerp, Belgium

Priyanka Shaw

Research group PLASMANT, Department of Chemistry, University of Antwerp, Universiteitsplein 1, B-2610 Antwerp, Belgium

Annemie Bogaerts

Plasma Bioscience Research Center, Applied Plasma Medicine Center, Kwangwoon University, Seoul, 01897, Republic of Korea

Eun Ha Choi

Department of Dentistry, Korea University Anam Hospital, Seoul, 02841, Republic of Korea

Jae Jun Ryu

Author Contributions: I.S. started, participated in the organisation of, and coordinated the study and wrote the article. E.C. participated in study design, researched data, and wrote the article. S.J. participated in study design and discussions. J.R. contributed to study design, researched data, and wrote the article. A.B. supervised the computational part of the study. M.Y. performed all simulations, analysed the simulation results, and prepared corresponding figures and tables. P.S. assisted in the simulations, participated in the discussion of the computational study. M.Y., P.S., and A.B. planned and wrote the computational part of the article. I.H.

684 contributed to the execution of the study, organised the database, accomplished the statistical analyses and
685 contributed to the drafting of the article. All authors read and agreed to the final version of the manuscript. J.R.
686 and I.H. are the guarantors of the present work, and, as such, had full access to all the data in the study, and take
687 responsibility for the integrity of the data and the precision of the data analysis.

688 **Corresponding authors:** Correspondence to Eun Ha Choi and Jae Jun Ryu

689 **Data Availability:** All data generated or analysed during this study are included in this published article (and
690 its supplementary information files)

691 **Competing Interests:** There are no competing interests to disclose.

692

693 **Table list**

694 **Table 1.** physical parameters of the DBD plasma source.

Gas source	**Air**
Available area of plasma discharge (mm^2)	3.8
Voltage (V_{rms}, kV)	1.69
Current (I_{rms}, mA)	9.6
Discharge voltage (kV)	0.2
On-time (ms)	25
Off-time (ms)	175
Cycle (μs)	31.4
Frequency (Hz)	31847.13376
Duty ratio on-time pulse (%)	13
Energy transfer/discharge cycle (J)	0.0000143
Energy transfer/continuous discharge (J/sec)	0.455
Energy transfer-/duty ratio (J/sec)	0.0569
Energy transfer of unit area/duty ratio ($J/sec \cdot mm^2$)	0.015

695

696

Supplementary Information

Enhanced Migration of Human Gingival Fibroblasts via Non-Thermal Biocompatible Dielectric Barrier Discharge Plasma

Ihn Han[1.2¶], In-Seok Song[3¶], Seung Ah Choi[4], Taebok Lee[5], Maksudbek Yusupov[6], Priyanka Shaw[6], Annemie Bogaerts[6], Eun Ha Choi[1*], and Jae Jun Ryu[3*]

[1]Plasma Bioscience Research Center, Applied Plasma Medicine Center, Kwangwoon University, Seoul, 01897, Republic of Korea

[2]Department of Plasma Bio-Display, Kwangwoon University, Seoul 01897, Korea

[3]Department of Dentistry, Korea University Anam Hospital, Seoul, 02841, Republic of Korea

[4]Division of Pediatric Neurosurgery, Pediatric Clinical Neuroscience Center, Seoul National University Children's Hospital, Seoul, 03080, Republic of Korea.

[5]Confocal Core Facility, Center for Medical Innovation, Seoul National University Hospital, Seoul 03082, Korea

[6]Research group PLASMANT, Department of Chemistry, University of Antwerp, Universiteitsplein 1, B-2610 Antwerp, Belgium

[*]Corresponding author: Eun Ha Choi, Ph.D.

Plasma Bioscience Research Center, Kwangwoon University, Gwangun-ro 20, Nowon-gu, Seoul, 139-701, Republic of Korea, Tel.: +82-2-940-5661, Fax: +82-2-960-5664; E-mail: ehchoi@kw.ac.kr

[*]Corresponding author: Jae Jun Ryu, DDS, MSD, PhD

Department of Prosthodontics, Korea University Anam Hospital, 73, Inchon-ro, Seongbuk-gu, Seoul, 02841, Republic of Korea, Tel.: +82-2-920-5423, Fax: +82-2-921-7348; E-mail: koprosth@unitel.co.kr

¶ These authors contributed equally to this work.

Index of figure and table

1. Supplementary materials and methods

1.1 Quantification of gene expression

The PCR amplification programme consisted of an initial denaturation at 95 °C for 3 min, followed by 45 cycles of denaturation at 95 °C for 10 s, annealing at 60 °C for 30 s, and extension at 72 °C for 10 s. The following primers were used: for MMP-2, forward, 5′-AAGAAGTAGCTGTGACCGCC -3′, and reverse, 5′- TTGCTGGAGACAAATTCTGG -3′; for VEGF, forward, 5′-CACACAGGATGGCTTGAAGA-3′, and reverse, 5′- AGGGCAGAATCATCACGAAG -3′; for Collagen type I, forward, 5′-CACACGTCTCGGTCATGGTA-3′, and reverse, 5′-AAGAGGAAGGCCAAGTCGAG -3′; for Collagen type IV, forward, 5′-

CTCCACGAGGAGCACAGC-3′, reverse, 5′-CCTTTTGTCCCTTCACTCCA-3′; for PDGF-beta, forward, 5′-CTGGCATGCAAGTGTGAGAC-3′, reverse, 5′-AATGGTCACCCGAGTTTGG-3′; for CDKN1A (p21), forward, 5′-AGTCAGTTCCTTGTGGAGCC-3′, and reverse, 5′-CATGGGTTCTGACGGACAT-3′; and for beta-actin, forward, 5′-CCTTGCACATGCCGGAG-3′, and reverse, 5′-GCACAGAGCCTCGCCTT -3′.

1.2 Immunoblot analysis

Briefly, total protein concentration in cell lysates was determined using the Pierce BCA Protein Assay Kit (Thermo Fisher Scientific, MA, USA). An equal amount of total protein (20 µg) was loaded on a (4–12) % gradient SDS-polyacrylamide gel for electrophoresis. The proteins were transferred onto a nitrocellulose membrane (Amersham™ Protran™ 0.2 µm NC, GE Healthcare Life Science, Buckinghamshire, UK). The membrane was blocked and incubated with the primary antibody at 4 °C overnight. After washing thrice with TBS containing 0.1 % Tween-20 (TBS-T), the membranes were incubated with secondary antibodies for 1 h at room temperature.

1.3 Computational simulation

We placed these model systems in a cubic box with dimensions ~8.5 × 8.5 × 8.5 nm^3 and solvated them by adding simple point-charge (SPC) [1, 2] water molecules together with a physiological (150 mM) concentration of NaCl. Afterwards, the systems were energy-minimised using the steepest descent method, followed by a series of equilibration runs with the following positional restraints: (a) positional restraints on the KD backbone atoms, a force constant of 10,000 $kJ.mol^{-1}.nm^{-2}$, and an NVT ensemble (i.e. constant number of particles, volume, and temperature) for 2 ns; (b) the same as in (a) but in an NpT ensemble (i.e. constant number of particles, pressure, and temperature); (c) the same as in (b) but a force constant of 1,000 $kJ.mol^{-1}.nm^{-2}$; and (d) the same as in (b) but a force constant of 200 $kJ.mol^{-1}.nm^{-2}$ for 6 ns. In this manner, we were able to slowly equilibrate the systems without causing strong disturbances in their original structures. Subsequently, we carried out the final equilibration simulations, again using the NpT ensemble for 200 ns (in the case of the native KD) and 750 ns (in the case of the oxidised KD), without any positional restraints.

2. Supplement results

We focused on Met and Cys residues for oxidation of the FAK protein, which are highly reactive amino acids (AAs). However, to find out which of the Met or Cys to oxidize, we calculated the solvent accessible surface area (SASA) of these residues. Thus, based on the SASA results we selected six AAs (i.e., Cys427, Met442, Cys559, Met571, Met617 and Met643) for oxidation, see AAs highlighted with light blue color in Table 1. As is clear, these residues have higher accessibility to solvent. To oxidize the above-mentioned AAs, we modified Met to methionine sulfoxide and Cys to cysteic acid (Figure S1).

Figure S1. Schematic illustration of the native and oxidized kinase domain (KD) of the FAK protein, together with its six amino acids (Met and Cys residues) selected for oxidation. The residues shown in the left and right figure are those before and after oxidation, respectively (see also Table S2).

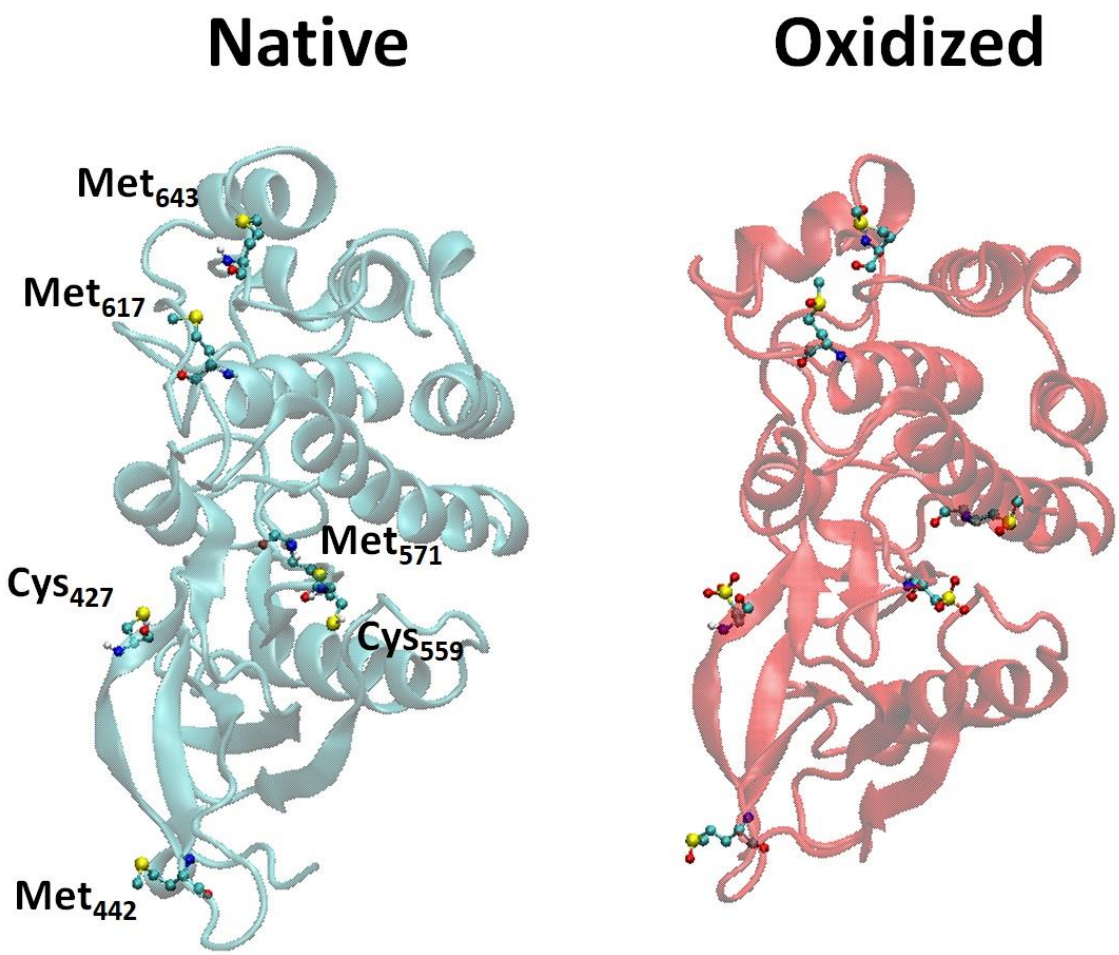

The percentage of the random coil structure increases, and the α-helix structure decreases by approximately 2-3 %, whereas other conformations stay more or less unchanged. This indicates that the oxidation results in a slight increase in the structural flexibility, thereby affecting its stability. Note that the oxidation degree used in our simulations is low, which probably corresponds to a short treatment time. Therefore, it does not lead to drastic conformational changes. However, it is most likely sufficient to change the function of FAK protein, thereby affecting its activity.

Figure S2. A slight conformational change and twisting in the FAK protein after oxidation.

Native

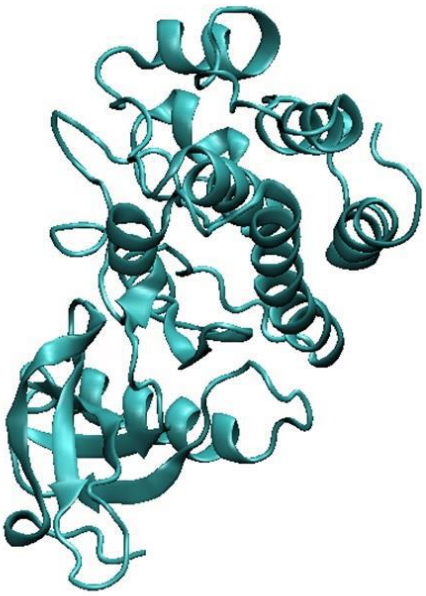

Oxidized

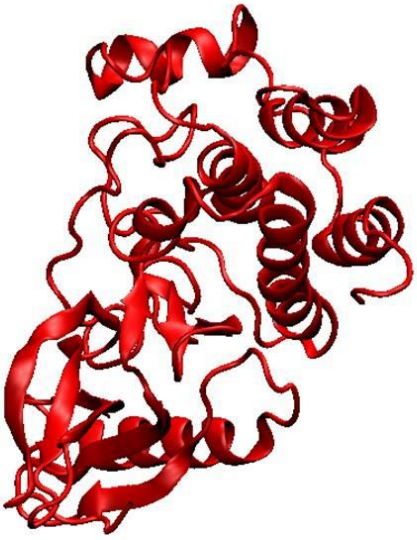

Native

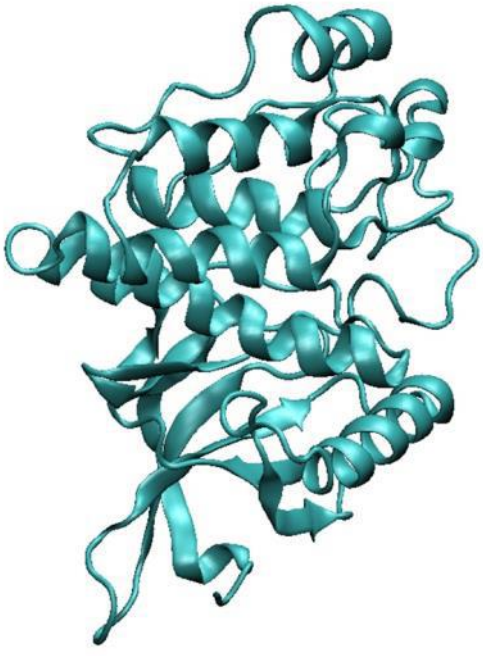

Oxidized

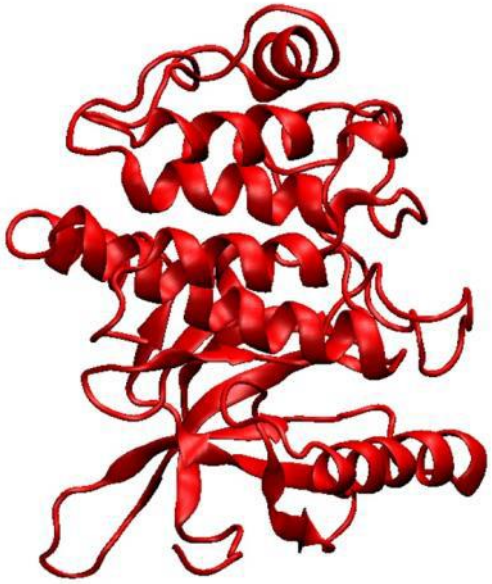

Figure S3. Zymography original blot. Clear areas represent proteolytic activity evaluated for NBP treatment on HGF cells. Lane 1, marker, lane 2, control, lane 3, NBP treated for 3 min.

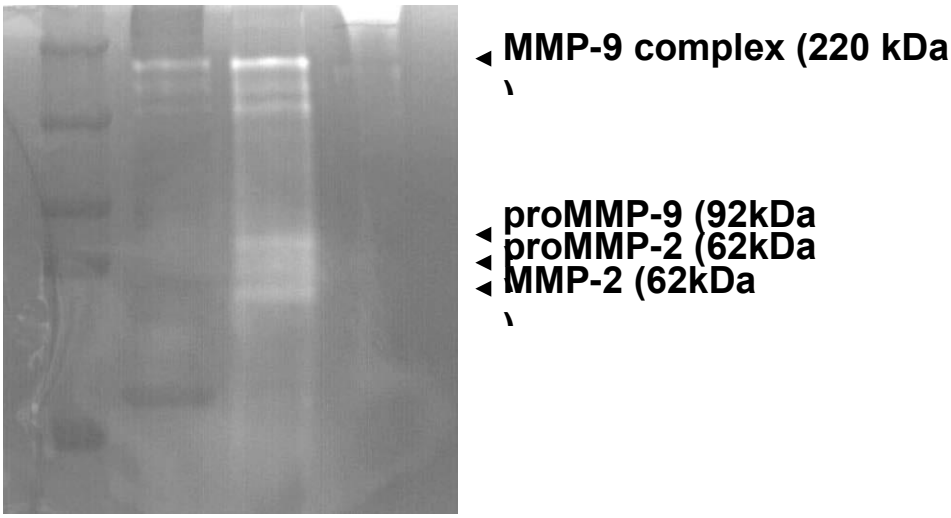

The native FAK reaches its equilibration after ~100 ns and stays stable in the rest of the simulation time, yielding an RMSD fluctuating around 0.43 nm. In contrast, the oxidized FAK protein obtains its stability at a much longer time, i.e., at around 600 ns, having a higher RMSD value than the native one, which fluctuates around 0.55 nm. This indicates that the oxidized structure become slightly more flexible than the native structure, which can be due to the conformational changes in the protein. Indeed, the secondary structure analysis showed a slight difference in secondary structure after oxidation (Table S2).

Table S1. Met and Cys residues of the KD of the FAK protein. Rows highlighted with light blue color show the residues that have higher SASA and are hence chosen for oxidation.

AA residue	Residue number	SASA (nm^2)
CYS	427	0.59 ± 0.14
MET	442	0.94 ± 0.16
CYS	456	0.04 ± 0.04
CYS	459	0.03 ± 0.03

MET	475	0.18 ± 0.10
MET	499	0.05 ± 0.05
CYS	502	0.02 ± 0.02
CYS	559	0.32 ± 0.09
MET	571	0.46 ± 0.16
MET	589	0.04 ± 0.04
MET	607	0.03 ± 0.03
CYS	611	0.02 ± 0.02
MET	612	0.02 ± 0.02
MET	617	0.44 ± 0.09
MET	643	0.99 ± 0.16
CYS	647	0.14 ± 0.08
MET	655	0.00 ± 0.00
CYS	658	0.00 ± 0.00

Table S2. Chemical structures of Met and Cys and their oxidized forms used for the creation of the oxidized KD of the FAK protein.

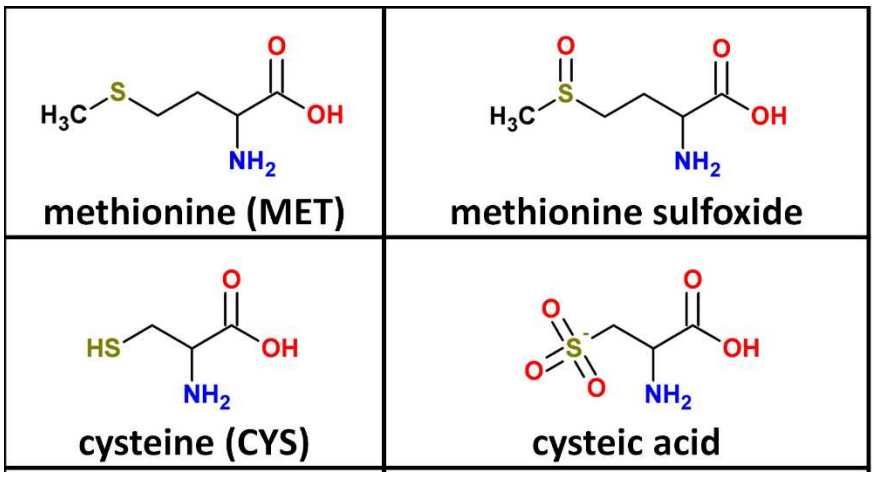

Table S3. Secondary structure analysis of the native and oxidized KD of the FAK protein.

System	Coil	β-sheet	β-bridge	Bend	Turn	α-helix	3-helix
Native	0.22 ± 0.02	0.15 ± 0.00	0.01 ± 0.00	0.13 ± 0.01	0.12 ± 0.01	0.35 ± 0.02	0.02 ± 0.01
Oxidized	0.25 ± 0.01	0.14 ± 0.01	0.01 ± 0.00	0.13 ± 0.01	0.11 ± 0.01	0.33 ± 0.01	0.02 ± 0.01

Reference

1 Berendsen, H. J., Postma, J. P. M., van Gunsteren, W. F. & Hermans, J. Interaction models for water in relation to protein hydration. In Pullman, B. (ed.) *Intermolecular forces*. The Jerusalem Symposia on Quantum Chemistry and Biochemistry, Vol. 14, 331–342 (Springer, 1981).

2. Hermans, J., Berendsen, H. J. C., Van Gunsteren, W. F. & Postma, J. P. M. A consistent empirical potential for water-protein interactions. *Biopolymers* **23,** 1513–1518 (1984).